CONF-760910--2

LBL-5757

Simultaneous Reactions at Disk and Porous Electrodes*

John Newman

Materials and Molecular Research Division, Lawrence Berkeley Laboratory, and Department of Chemical Engineering, University of California, Berkeley, California 94720

November, 1976

Abstract

Advances in electrochemical engineering are reviewed, and the methodology of the analysis of electrochemical systems is outlined. Examples illustrative of current research concern simultaneous reactions for flow-through porous electrodes and the more fundamental system of a rotating-disk electrode. Here the undesirable side reaction is the formation of dissolved hydrogen, and the main reaction is the deposition of copper from sulfuric acid solutions. Distributions of reaction rate, concentration, and potential describe the detailed system behavior. The side reaction is responsible for the poorly defined limiting-current plateau on the disk electrode and provides a limit for the maximum flow rate at which good recovery can be achieved with the porous electrode.

*Plenary lecture presented at the 27th Meeting of the International Society of Electrochemistry at Zürich, Switzerland, September 6, 1976.

DISCLAIMER

Electrochemical Engineering

We should like to begin this conference with a definition of electrochemical engineering. Please realize that many of us have our individual concept of the scope of the field. In an attempt to avoid generating controversy, I shall emphasize the thoughts of Wagner.[1] He says that electrochemical engineering deals with the problem of scale up -- that is, the design of commercial systems from laboratory data. We should get the impression that we can focus attention on a certain length, characteristic of the cell in question.

Other definitions of electrochemical engineering can come to mind. For example, it might encompass the conception, design, and optimization of electrode processes. Or it could involve the synthesis of known principles and processes for useful purposes. Or it could be stated that the central theme is the treatment of complete systems, including the many factors which find simultaneous importance in practical operations.

Wagner also laid down a specific program whereby one should carry out the general objectives of electrochemical engineering. Central to the effort toward scale up of processes is the role of theoretical calculations confirmed by experiments. We should never neglect the powerful influence which the application of this basic premise of the scientific method can have in the rapid progression of science and technology. We should expect to see this principle applied in day-to-day investigations, not just to revolutionary advances such as the wave-particle duality of matter. We can be particularly delighted when both of these important steps -- theory and experiment -- can be included in an individual study and its subsequent report.

In some cases, the system is too complex to permit convenient theoretical calculations. Then the approach of electrochemical engineering can be useful first in the identification of relevant variables and second in the development of empirical correlations. We might cite as examples here the characterization of mass transfer with rotating cylinders in turbulent flow, mass transfer in free convection, and mass transfer with simultaneous evolution of gas bubbles.

In reading his paper, we feel that Wagner is defining electrochemical engineering in its distinction from electrochemistry. He emphasizes that the electrochemical engineer is supposed, in carrying out his work, to draw upon all the fundamentals of electrochemistry. In particular, he mentions Faraday's law, electrolytic dissociation and conduction, the thermodynamic treatment of the potential of galvanic cells, and electrode kinetics.

Wagner distinguishes two principal problem areas for detailed treatment, and indeed much of the effort in electrochemical engineering can be fruitfully regarded on the basis of this classification.

The first basic problem is mass transfer, principally by means of convection and diffusion. Here he cites work on free convection in laminar flow at a vertical electrode. The problem of scale up is exemplified by the fact that the limiting current density is inversely proportional to the one-fourth power of the distance from the leading edge of the electrode. In terms of the identification of relevant variables, he points out that this conclusion can be reached by a contemplation of the governing equations even though their detailed

solution to obtain the coefficient multiplying the distance factor is not trivial.[2] Experimental confirmation and empirical correlation were achieved quite early.[3]

The second basic problem area Wagner identifies as one of potential distribution -- applications of potential theory according to solutions of Laplace's equation, applicable in the absence of concentration variations. How does the current density depart from the primary distribution to yield a finite value at the edge of an electrode? An important problem of scale up is involved here, governed by the ratio of the solution conductivity κ to the slope $di/d\eta$ of the polarization curve of electrode kinetics and a characteristic length L of the system. Even at the time of this conference, the International Union of Pure and Applied Chemistry is taking steps to designate $\kappa/L(di/d\eta)$ as the polarization parameter or Wagner number.

From these examples, it is apparent that relating electrochemical engineering with scale up puts an emphasis on the transport processes of conduction, diffusion, migration, and convection, whereas electrochemistry deals primarily with electrode processes at the surface itself.

While all the transport processes do occur simultaneously and can sometimes be treated simultaneously, the two basic problem areas identified by Wagner deal with two limiting cases which provide a convenient basis for defining the behavior expected in a specific electrode geometry. Consider two electrodes in the walls of a flow channel, as depicted in figure 1. Figure 2 represents the current density distribution along the upper cathode (facing downward so that natural convection

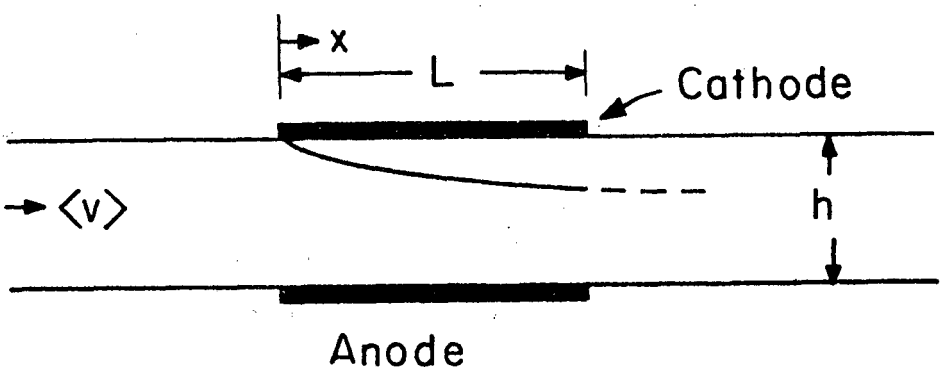

XBL-673-2382A

Figure 1. Plane electrodes in the walls of a flow channel.

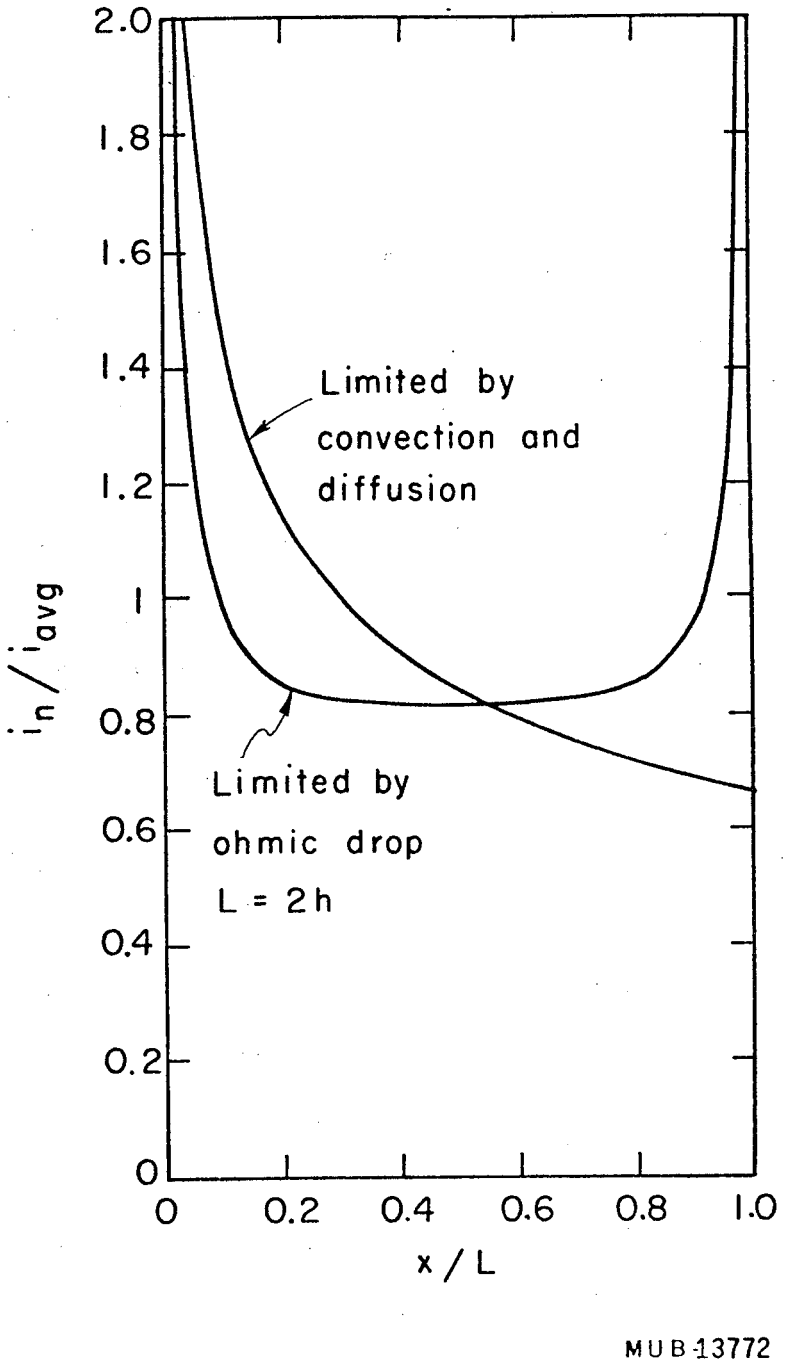

Figure 2. Current distributions along an electrode embedded in the wall of a flow channel.

will have a minimal effect on the flow pattern). The curve labeled "limited by convection and diffusion" decreases continuously from the left to the right along the electrode. The current density is high -- even infinite -- at the left where fresh solution reaches the electrode and decreases toward the right as the solution becomes depleted while flowing along the electrode. The distribution is independent of the position of the counterelectrode. The curve labeled "limited by ohmic drop" applies in the absence of significant concentration variation and electrode surface overpotential and is symmetric because the counter-electrode is symmetrically placed on the opposite wall of the flow channel. This distribution is independent of the flow pattern, as long as there is sufficient convection to eliminate concentration variations. However, it does depend on the placement of the counterelectrode, including its distance. (For this example, $L = 2h$.) The current density is high near the edges of the electrode because of the close spacing of the equipotential lines in this region, as shown in figure 3, and the fact that the current can flow through the solution in the channel beyond the electrodes and can approach the electrode edge from a larger range of angles than for other points along the electrode surface.

The average current density, with which the curves are normalized, also depends upon quite different quantities for the two cases in figure 2. For the ohmically limited curve, the average current density is proportional to the potential difference applied between the electrodes and inversely proportional to the ohmic resistance of the system. This implies a proportionality to the solution conductivity, an inverse dependence on the length characteristic of the system, and a quite different value for

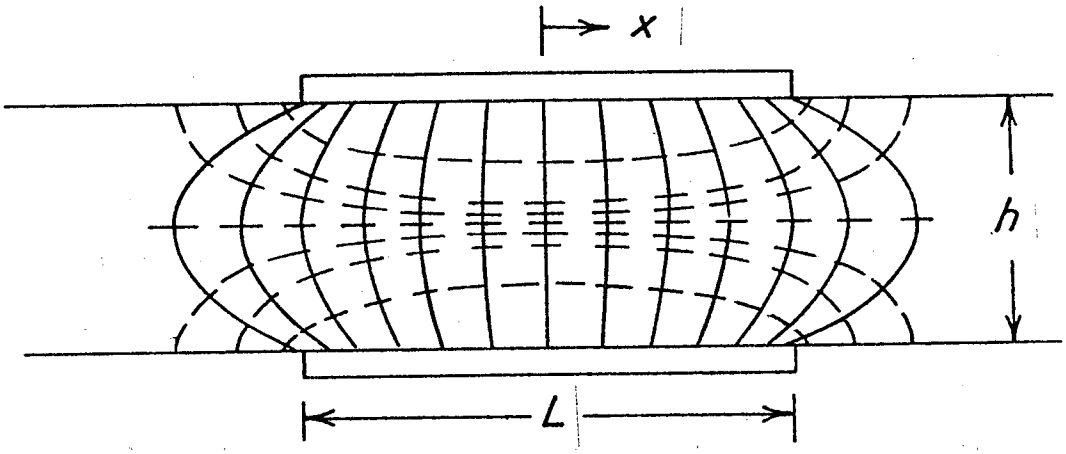

XBL7110-4608

Figure 3. Sketch of current lines (solid) and equipotential surfaces (dashed) for electrodes opposite each other in insulating planes.

a different placement of the counterelectrode. On the other hand, the average current density limited by diffusion and convection is proportional to the bulk concentration of reactant, the cube root of the flow rate, and the two-thirds power of the diffusion coefficient and is inversely proportional to the cube root of the electrode length in the direction of flow.

A considerable body of literature deals with these limiting cases where the current distribution is determined by convection and diffusion on the one hand or by ohmic potential drop and surface overpotentials on the other hand. It is a significant advance that the distribution determined by all these factors simultaneously can now be calculated for a number of situations. Parrish and Newman treated two electrodes in the walls of a flow channel,[4] as depicted in figure 1, and also the simpler case of a short electrode in a wall with tangential flow.[5] For these situations, the primary distribution and the limiting current distribution are similar to those shown in figure 2, and one can imagine how the distribution below the limiting current shows simultaneously the influence of inhibited mass transfer, ohmic potential drop, and electrode polarization.

The rotating disk electrode[6,7] is characterized by a uniform limiting current density and a nonuniform primary distribution (see figure 4). The rotating sphere[8] in figure 5 shows behavior intermediate between the uniform primary distribution and the mildly nonuniform limiting distribution. Free convection in a rectangular cell, treated by Asada et al.,[9] is another example with a uniform primary distribution and a nonuniform limiting current distribution (see figure 6). Alkire

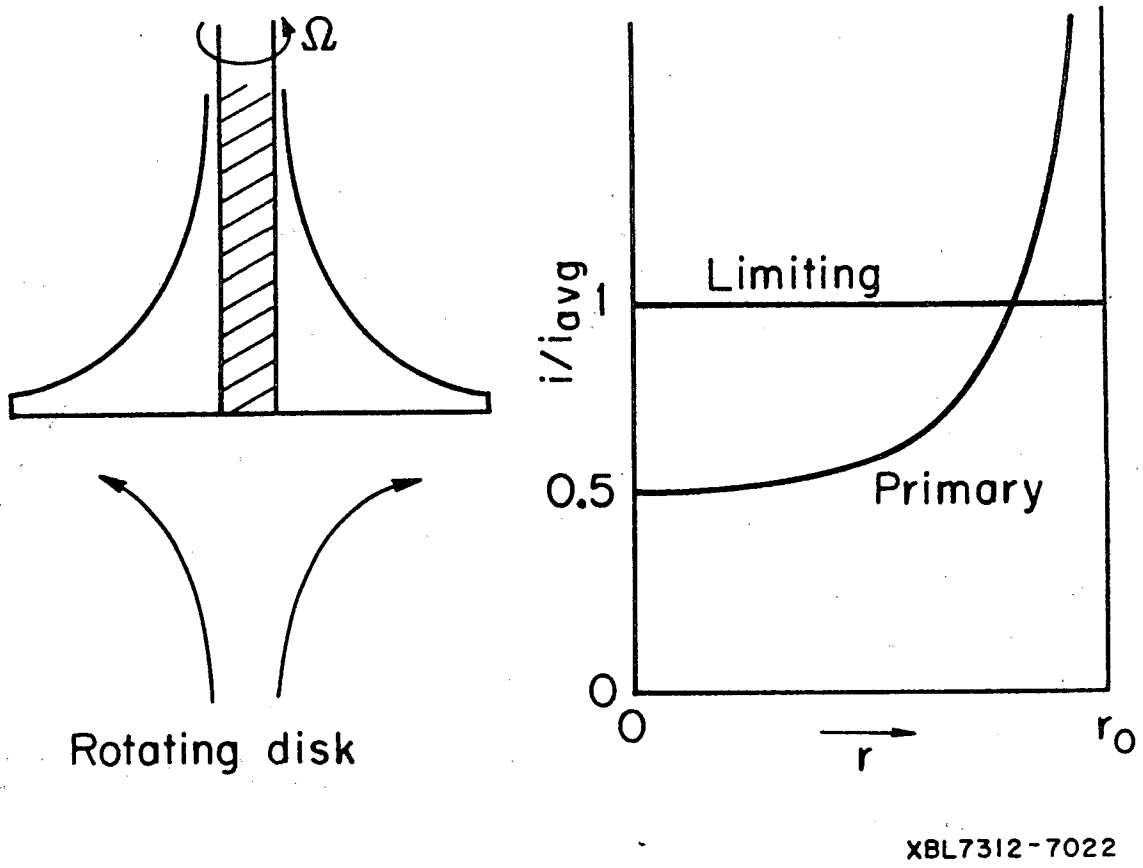

Figure 4. System schematic and current distributions for a rotating disk electrode.

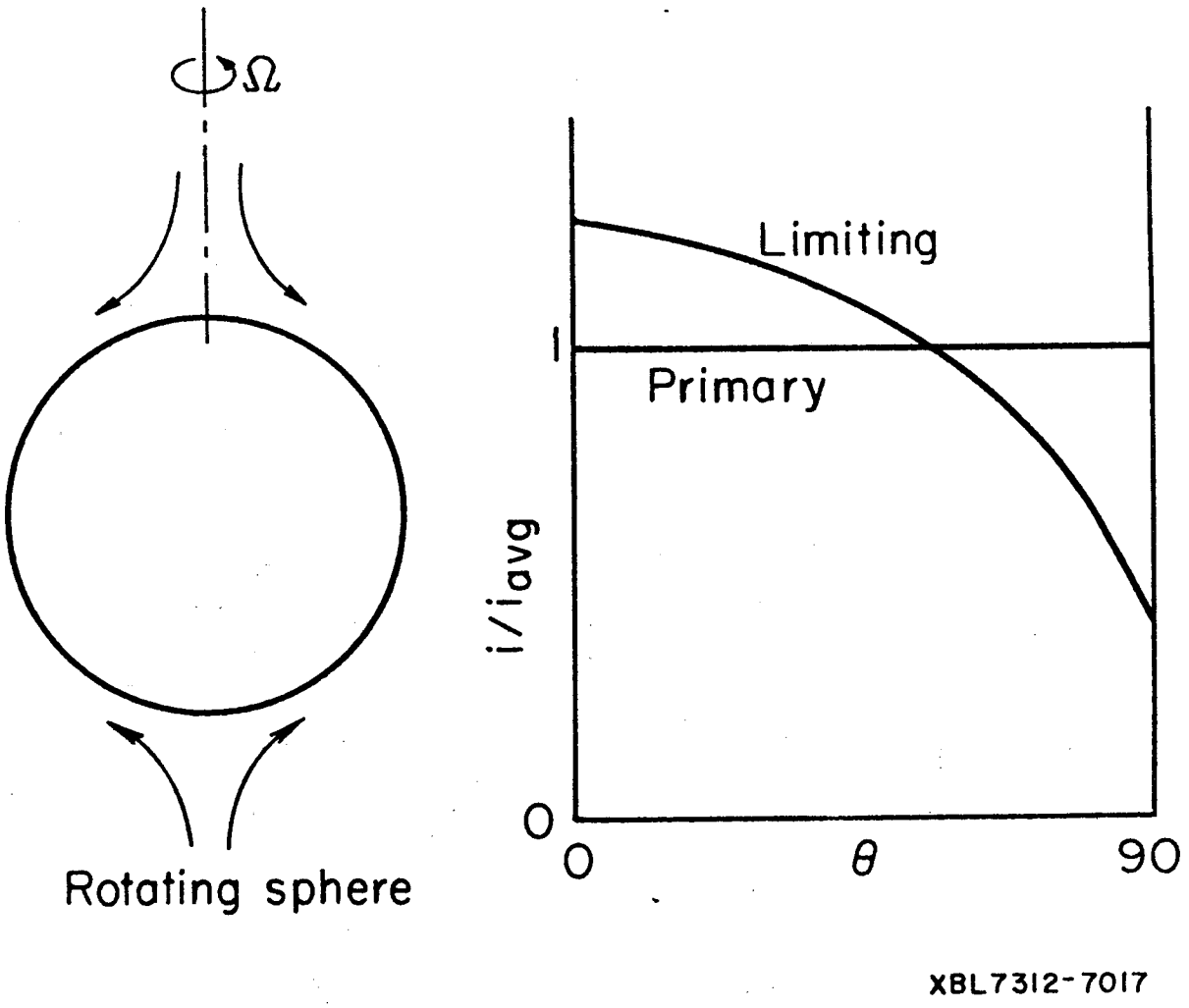

Figure 5. System schematic and current distributions for a rotating spherical electrode.

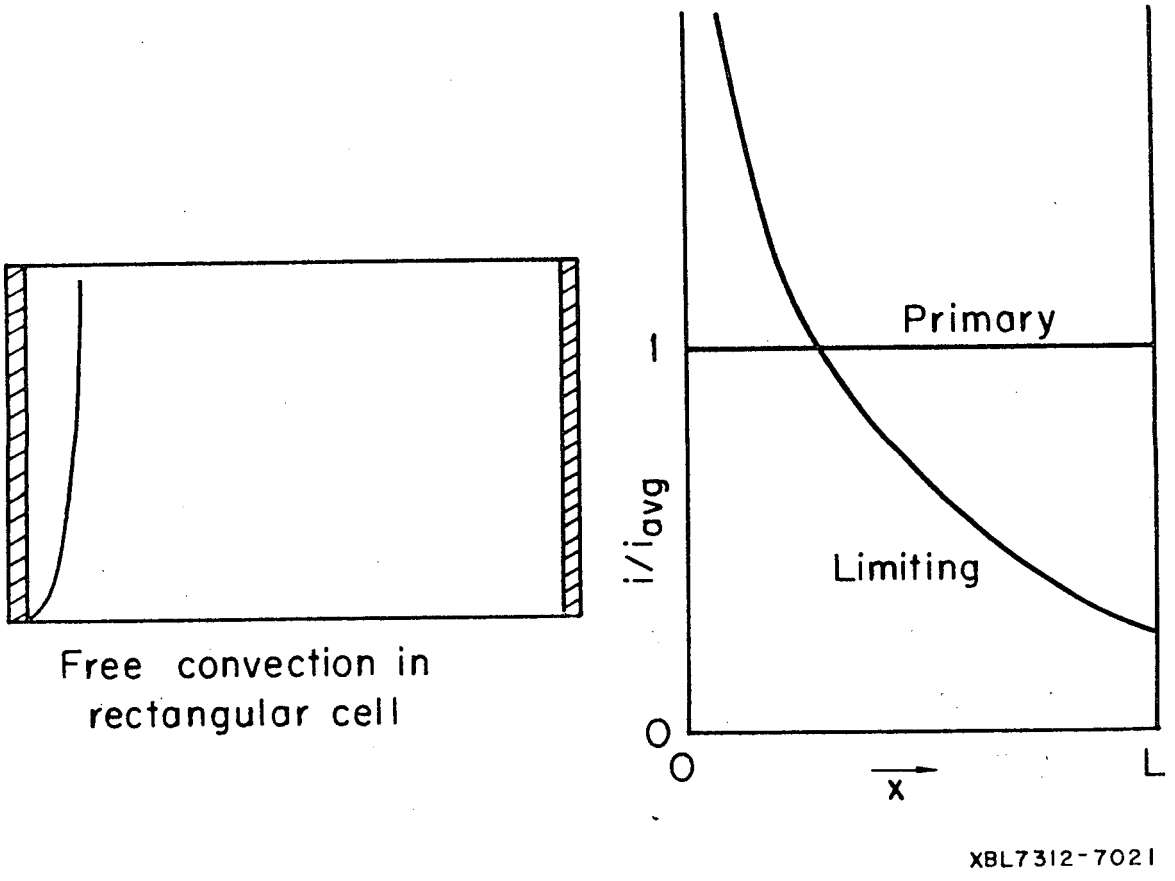

Figure 6. System schematic and current distributions for electrodes comprising the ends of a rectangular cell.

and Mirarefi[10] calculated the intermediate distribution on a tubular electrode with the counterelectrode either downstream (figure 7) or upstream.

One is generally optimistic that these complex intermediate distributions can be calculated for any geometry for which the limiting cases of the primary distribution and the limiting current distribution can be obtained separately.

Flow-through Porous Electrodes

As examples of current research efforts to develop electrochemical engineering in terms of theoretical calculations confirmed by experiments, we should like to discuss the treatment of simultaneous reactions in flow-through porous electrodes and, in a later section, at a rotating-disk electrode.

Flow-through porous electrodes show promise in a number of applications, such as:

1. Metal ion recovery or removal from aqueous solution. Copper, mercury, and silver have been removed successfully, and gold should be no problem. Lead is more difficult to remove because of its greater electronegativity.

2. Oxidation of organic pollutants and cyanide ion.

3. Electro-organic synthesis. For example, adiponitrile is produced by the dimerization of acrylonitrile.

Several flow arrangements for a pair of flow-through porous electrodes are depicted in figure 8. Configuration a has been used for removal of copper ions. It could also be used in a flow redox system for energy

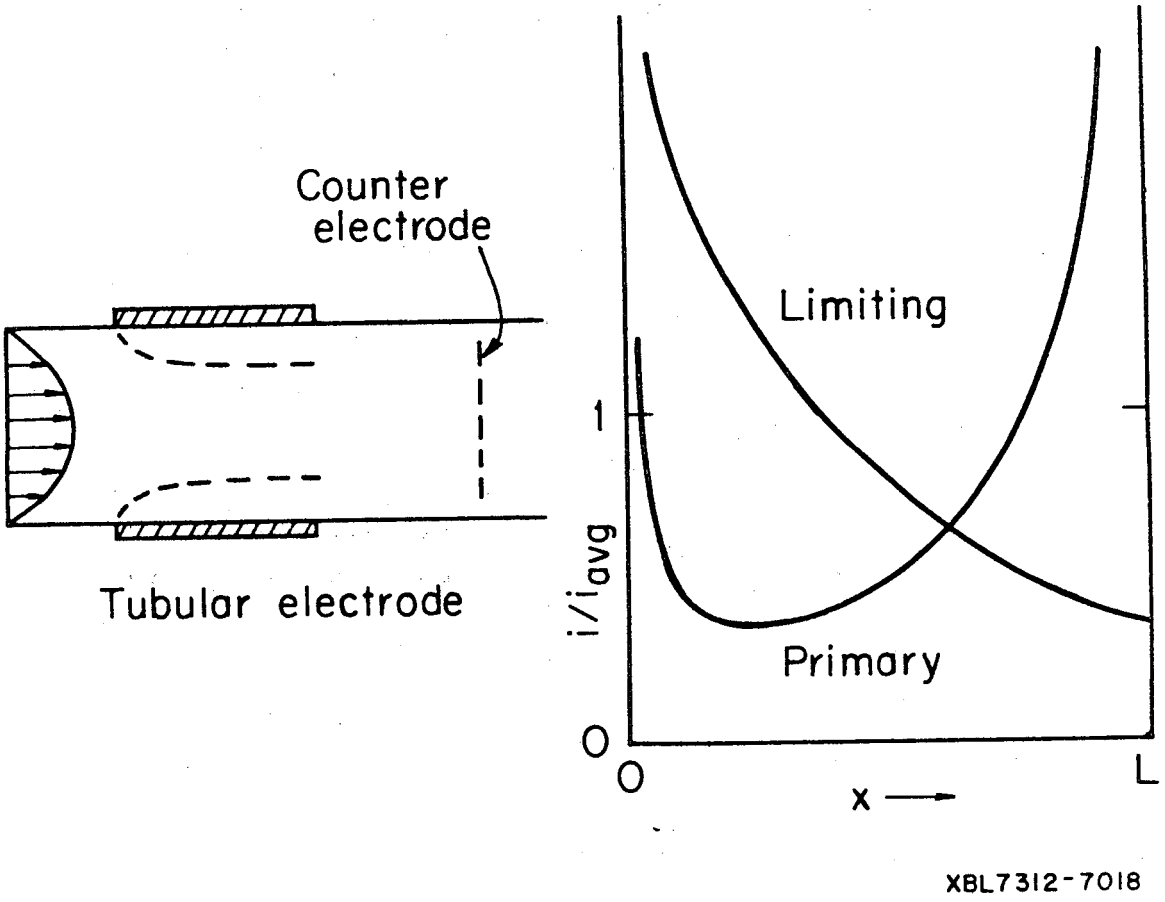

Figure 7. System schematic and current distributions for a short tubular electrode.

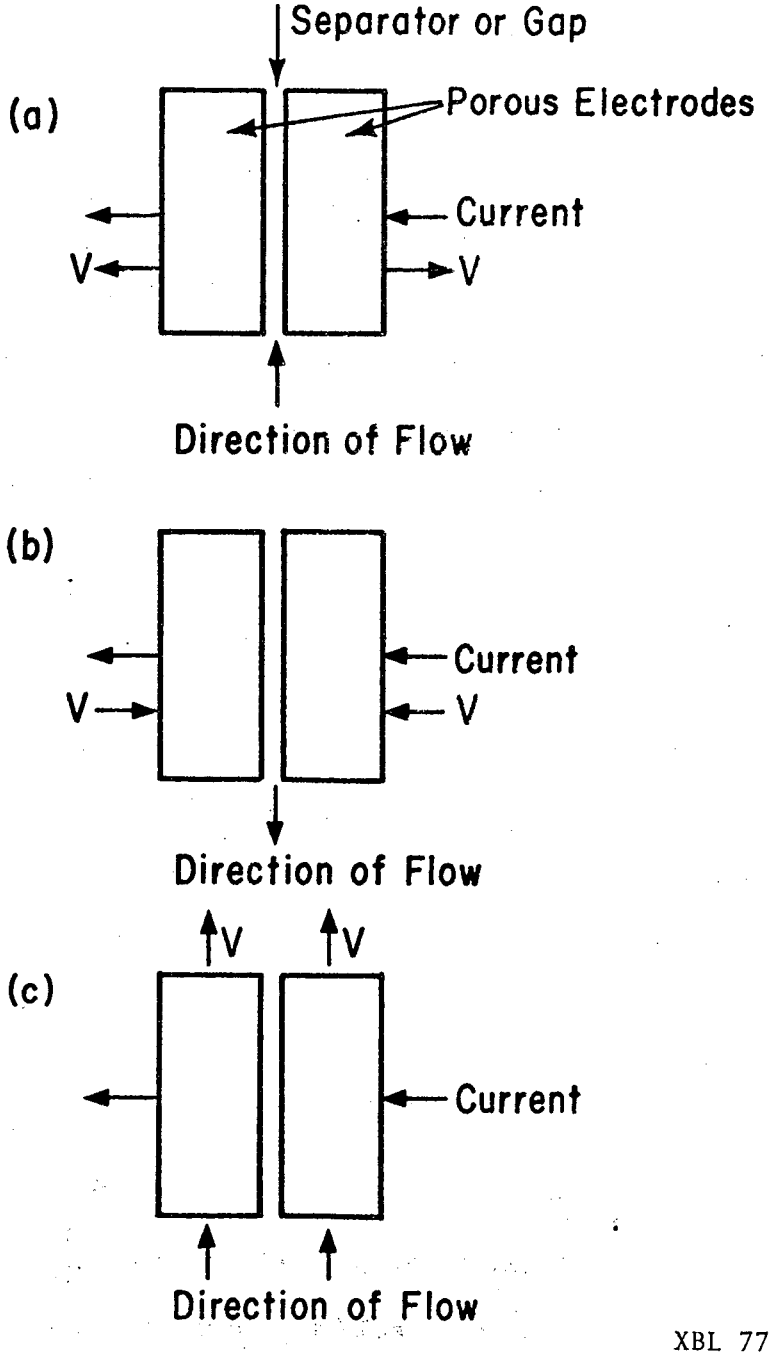

XBL 771-7116

Figure 8. Various configurations of electrode placement relative to the direction of fluid flow.

storage. The feed could contain Fe(II) and Ti(IV). On charging in configuration a, the Fe(II) would be oxidized to Fe(III) in the anode while Ti(IV) would be reduced to Ti(III) in the cathode. These oxidized and reduced solutions would flow to separate storage tanks. To recover the energy, the flows would be reversed and configuration b would apply. It would be interesting to see what faradaic efficiency could be achieved in practice in a cell without a separator, since the unreacted Ti(III) and Fe(III) would be lost according to the reaction

$$Ti(III) + Fe(III) \rightarrow Ti(IV) + Fe(II) \qquad (1)$$

when the streams are allowed to mix after flowing through the porous electrodes. Configuration c may permit a high flow rate because the applied potential difference applies along its entire length, undiminished by the ohmic potential drop in solution which would exist in configurations a and b. However, the one-dimensional situations are easier to analyze.

Porous electrodes do not generally permit the separate treatment of the limiting cases discussed in the last section. Here we should expect to require simultaneous treatment of mass-transfer limitations to the wall from the flowing solution, ohmic potential drop through the thickness of the electrode, heterogeneous reaction kinetics, and (in the present analysis) the existence of a side reaction. The problem of scale up is as critical for porous electrodes as in other areas of electrochemical engineering. The basic equations for describing these factors are outlined in the next section.

For the problems considered here, the main reaction is the deposition of copper, and the side reaction is the generation of dissolved hydrogen. We hope to keep the hydrogen in solution so that the velocity profile will not be disturbed. Figure 9 shows the reaction distribution through the thickness of the porous electrode. The conditions chosen are close to the limiting current for the deposition of copper. Consequently, the reaction rate for the primary reaction decreases in an almost exponential manner with distance, as the solution is depleted in copper while flowing through the electrode. The side reaction, generation of hydrogen, responds mainly to the electric driving force between the solid matrix and the electrolytic solution. Its rate is high near the entrance to the porous electrode and drops to a nearly constant value near the rear. The reason for this can be seen in figure 10, which represents the variation in the solution-phase potential Φ_2 for a counterelectrode placed upstream of the working electrode, as in configuration a of figure 8. The matrix has a high conductivity, and its potential Φ_1 is nearly constant. The solution potential Φ_2 varies little near the rear because the current carried in the solution is small in this region.

The local current efficiency actually goes through a slight maximum near $x/L = 0.18$ in figure 9. The current efficiency is low at the entrance because the high electric driving force leads to a relatively high rate for the side reaction. For somewhat larger values of x, the side reaction decreases more rapidly than the primary reaction, and the local current efficiency rises. However, the primary

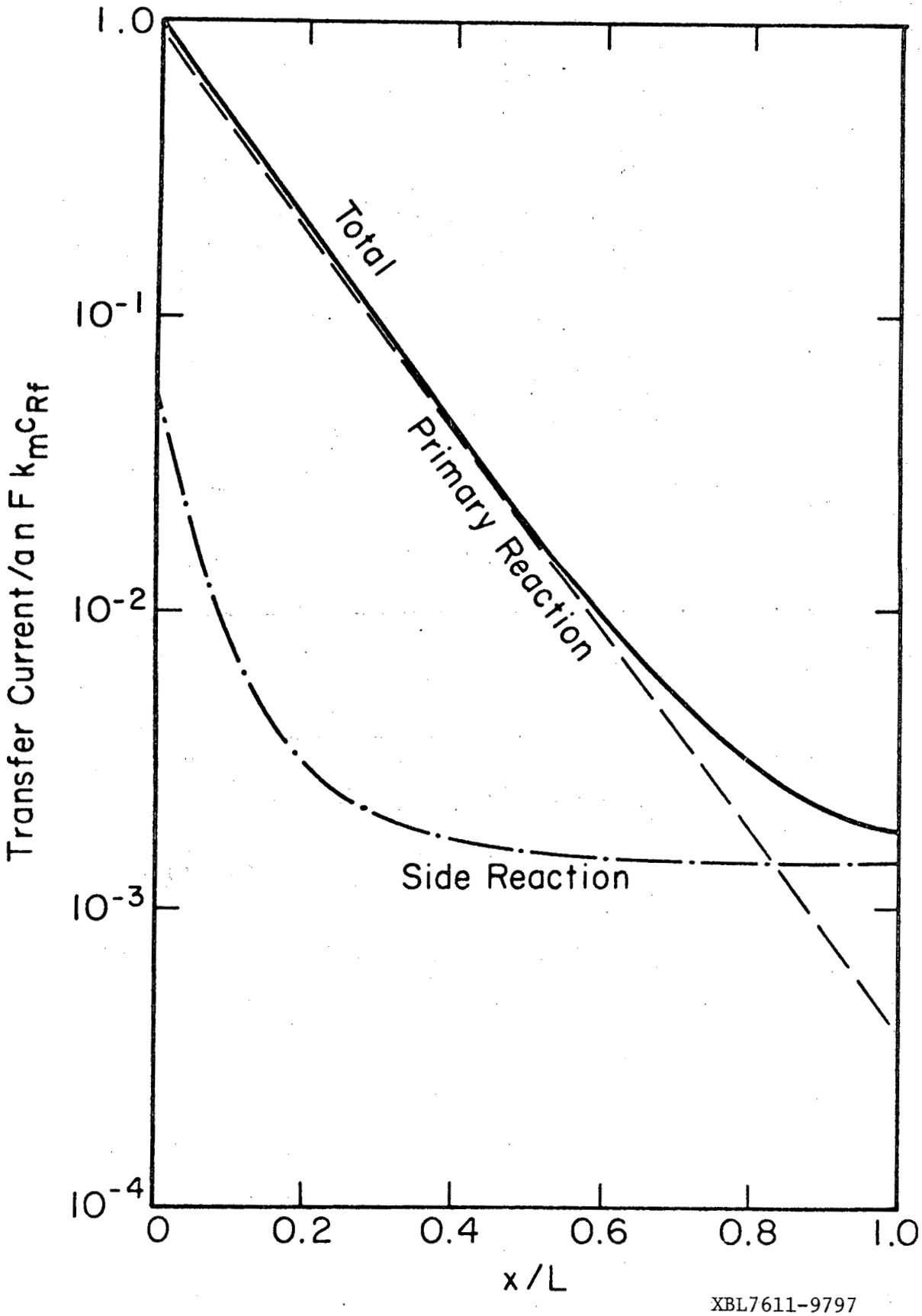

Figure 9. Current distributions for deposition of copper and generation of dissolved hydrogen within a porous electrode with fluid flow from left to right, calculated for v = 0.003328 cm/sec, a = 25 cm^{-1}, ε = 0.3, L = 6 cm, c_{Rf} = 0.0105 mole/ℓ, and VOP = -0.403 V relative to a calomel reference electrode in the dilute-product stream.

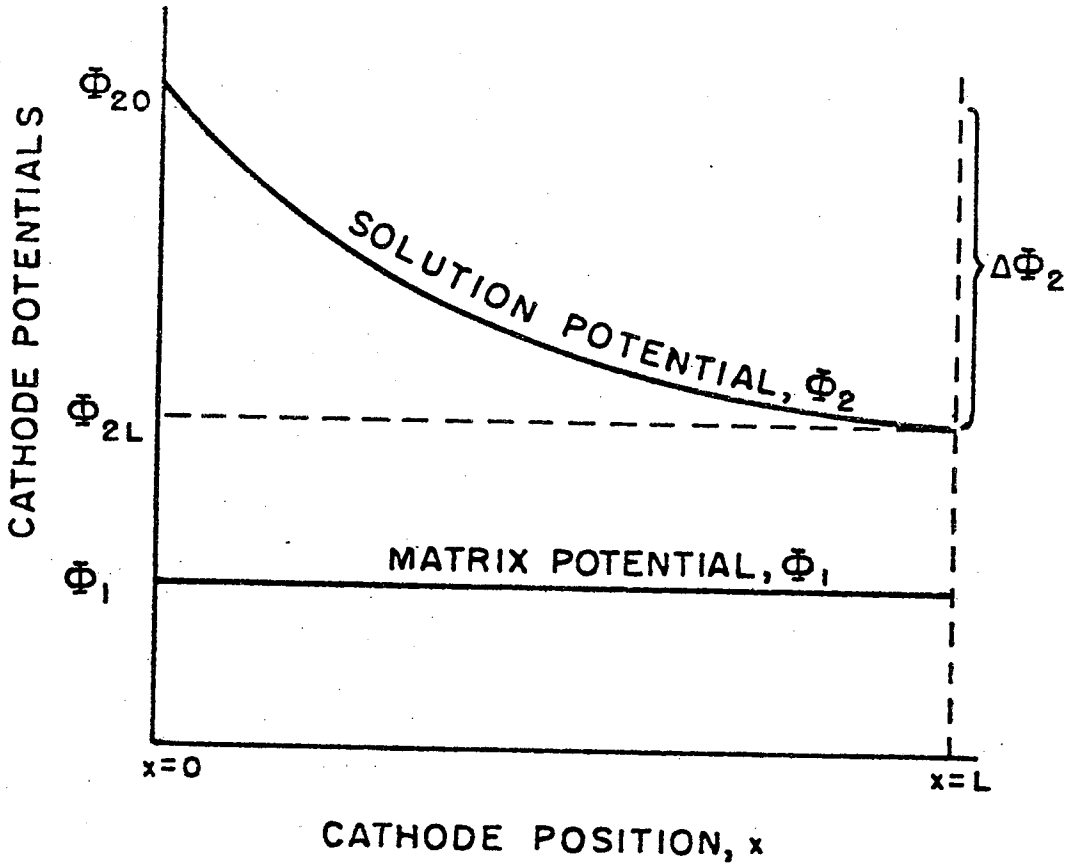

Figure 10. Solution-phase and solid-matrix-phase potentials, as functions of cathode position.

reaction rate continues to decrease with distance because of the depletion of copper ions, and consequently the local current efficiency eventually drops to about 23 percent at the rear of the electrode. One might well ask, "Why not eliminate the last 40 percent of the thickness of the electrode?"

Figure 11 shows the concentration of copper ions through the thickness of the electrode. The high electric driving force at the entrance results in a very low wall concentration there. As the electric driving force decreases with x, the wall concentration rises toward the bulk value. With the diminishing reaction rate through the next part of the electrode, the wall concentration is able to decrease also, despite the smaller electric driving force in this region. We can also see from this figure that the bulk concentration is depleted by an additional factor of 20 in the last 40 percent of the electrode, despite the lowered current efficiency in this region. This additional metal ion removal can be achieved with relatively little additional expense for the added electrode thickness and virtually no added cost due to added ohmic potential drop.

In figure 12 we show a detailed comparison between model calculations and the experimental results of Bennion and Newman.[11] Not only are the current-potential curves compared, but also the effluent copper concentrations (in mg/ℓ) are shown beside the experimental and theoretical data points. The agreement should be regarded as satisfactory.

Incidentally, the calculated results in figures 9 and 11 correspond to the upper curve in figure 12, that is, at a superficial velocity of 0.003328 cm/sec, and are at a potential of VOP = -403 mV with a calculated effluent concentration of 0.28 mg/ℓ.

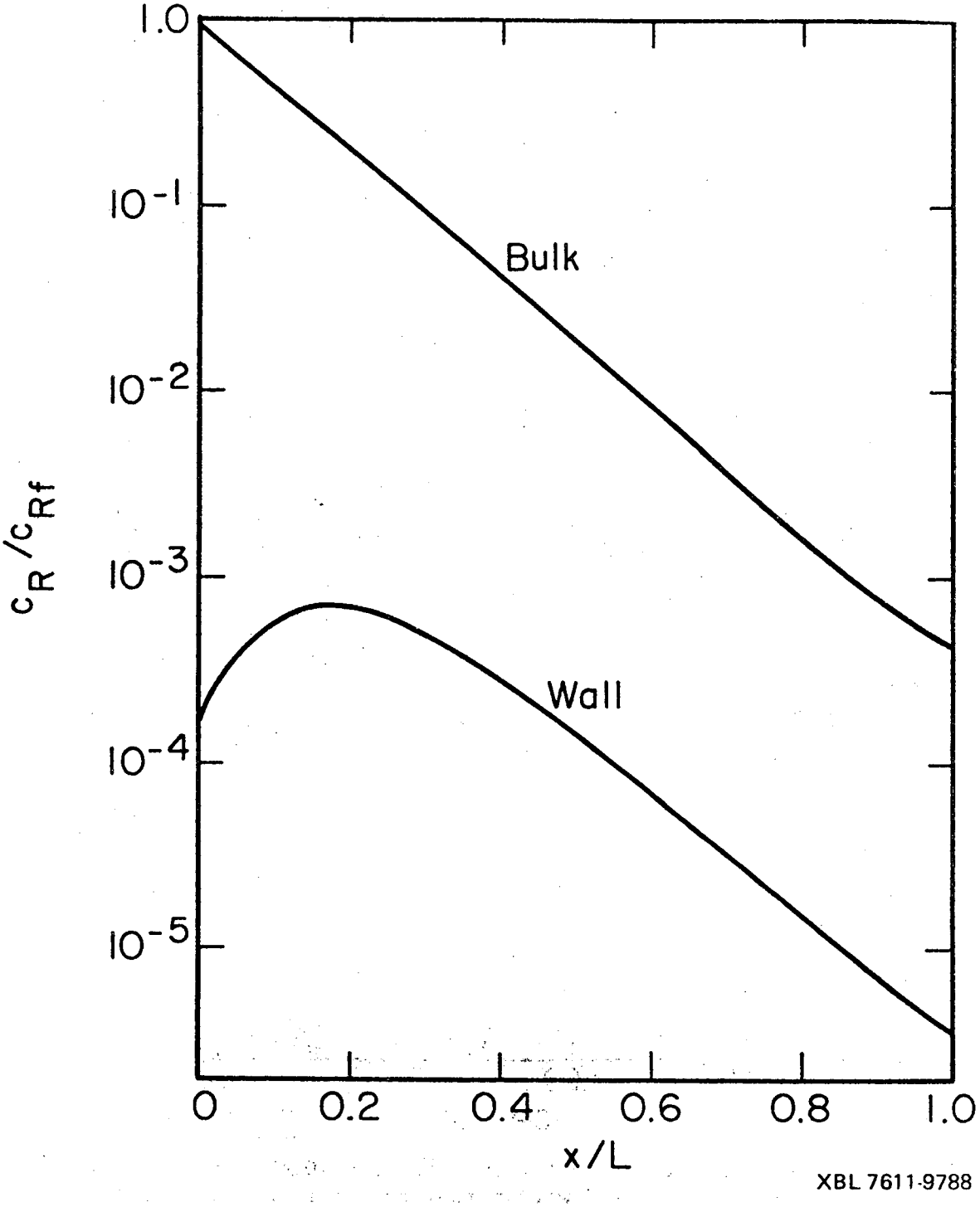

Figure 11. Distribution of copper concentration in the flowing stream and along the pore wall, for the conditions of figure 9.

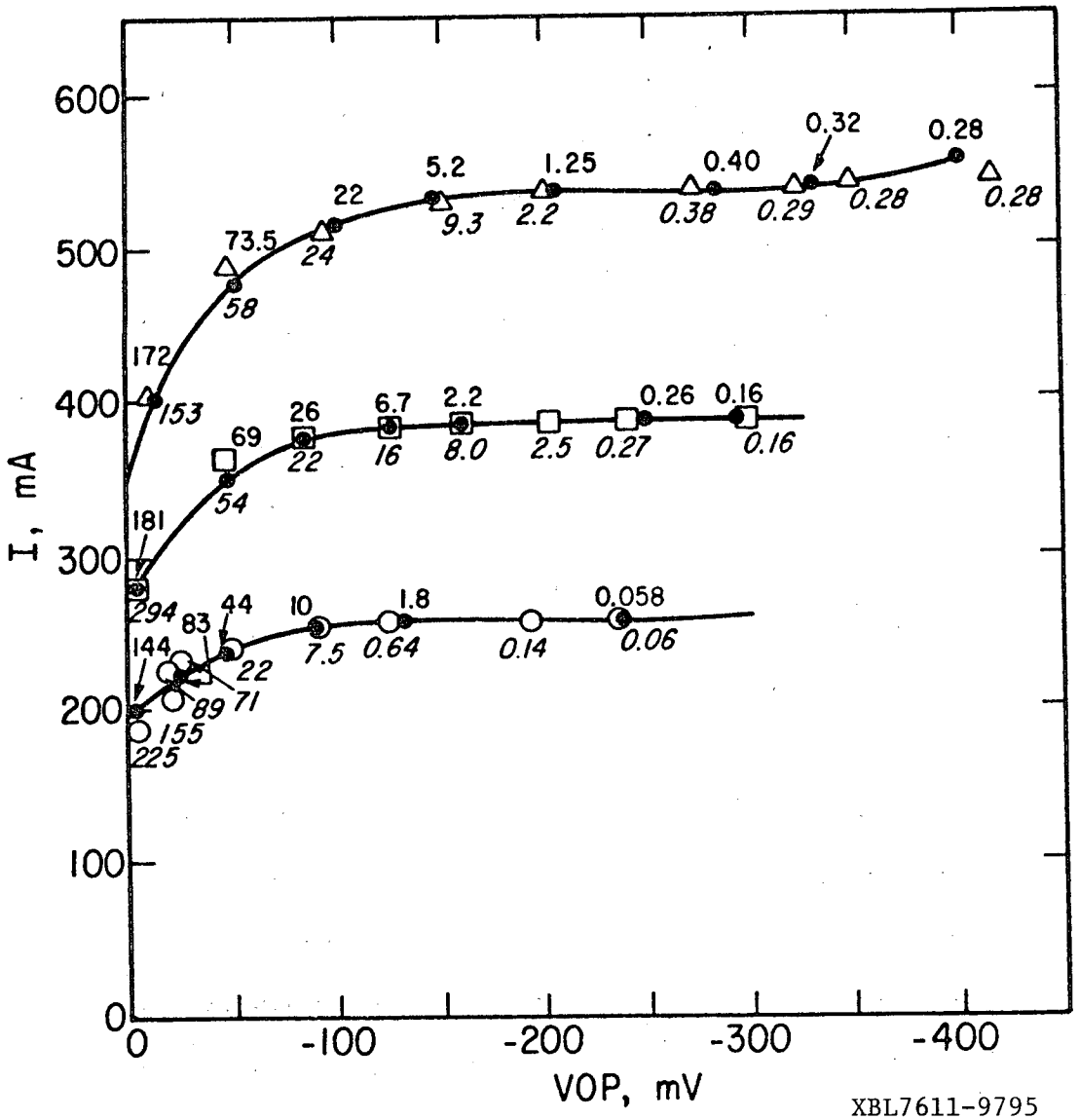

Figure 12. Current-potential curves for an electrode 10.1 cm in diameter and 6 cm deep,[11] packed with porous carbon flakes and chips. Open symbols are experimental data points; closed symbols are calculated. Calculated effluent concentrations (in mg/ℓ) are indicated above the corresponding points in upright type; experimental values are given in *italic* type below the corresponding data points. The flow rate was 8 cm^3/min for the circles, 12 cm^3/min for the squares, and 16 cm^3/min for the triangles.

The principal parameters adjusted to ensure agreement between the calculated and experimental values in figure 12 are the mass-transfer coefficient k_m and the exchange current densities of the principal and side reactions. The values of k_m are determined mainly by the effluent concentrations toward the right on the experimental curves, and the value of the exchange current density for copper deposition is governed by the current values toward the left. The exchange current density for hydrogen generation attempts to fit the rise of the curves above the apparent limiting current and the observed onset of hydrogen evolution.

The fitted values of k_m for the three curves on figure 12 are displayed by means of open triangles on figure 13 in the form of a correlation of the dimensionless Sherwood number $\varepsilon k_m/aD_o$ in its dependence on the dimensionless Péclet number v/aD_o. At the low Reynolds numbers $v/a\nu$ used here, the local fluid velocity should be everywhere proportional to the superficial velocity v, and there should be no separate dependence on the Schmidt number ν/D_o when the results are plotted in the manner of figure 13. However, there will be a dependence on the detailed geometry of the porous electrode, characterized partially by the void volume fraction or porosity ε, and it is felt that there will be also a dependence on the electrode thickness as characterized by aL. Figure 13 is an example of a dimensionless empirical correlation, alluded to by Wagner as one of the useful tools of electrochemical engineering.

The data of Bennion and Newman show a clear proportionality of k_m to the 0.5475 power of the velocity. Unfortunately, there is an

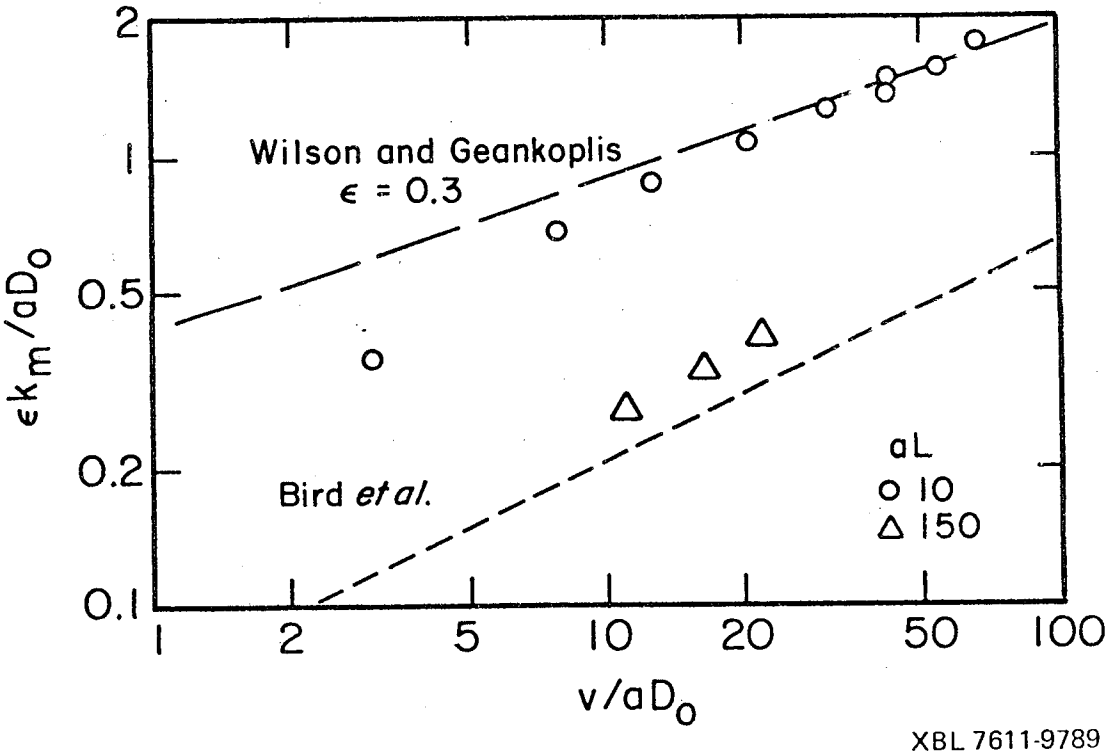

Figure 13. Correlation of the Sherwood number as a function of Péclet number and dimensionless electrode thickness aL. Open triangles come from a fit of the data of figure 12; open circles are the results of Appel and Newman.[12] Two correlations from the literature are also shown.

uncertainty in the specific interfacial area of the electrode used. The value of a may actually be higher by a factor of 4 to 12 than the value of 25 cm^{-1} used in the treatment of the data.[13]

Additional calculations at higher superficial velocities confirm the observation that the cell cannot be operated in these ranges without loss of the limiting-current plateau and extensive interference by the side reaction. In harmony with the quantitative design principles,[11] these calculations show that an increase in the superficial velocity increases the ohmic potential drop in the solution so that there is either excessive side reaction at the entrance to the porous electrode or a failure to maintain the limiting-current condition near the exit. A decrease in the feed concentration will also increase the side reaction relative to the primary reaction and cause the limiting-current plateau to become less distinct. The ability to calculate the current distributions below the limiting current and in the presence of a side reaction permits one to determine the economically optimum operating conditions and even permissible operating conditions when the side reaction accounts for a substantial fraction of the total current, and there is a penalty for making the electrode thicker because the side reaction does not necessarily decrease with increasing distance through the electrode.

Governing Equations

While we don't go into any details of analysis here, it may be useful to record some of the fundamental equations we use. In this way one can perceive just what physical phenomena are being described. It may also be apparent where improvements in the description would be fruitful. Equations for porous electrodes are treated elsewhere[14,15] with different degrees of detail and generality.

The laws of transport in dilute electrolytic solutions have been known for many years. The flux density of a species is due to migration in an electric field, diffusion in a concentration gradient, and convection with the fluid velocity:

$$\underline{N}_i/\varepsilon = -z_i u_i F c_i \nabla\Phi_2 - D_i \nabla c_i + c_i \underline{v}/\varepsilon \ . \qquad (2)$$

A material balance for a small volume element leads to the differential conservation law which states that the time rate of change of the concentration of species i is equal to its net input plus production:

$$\frac{\partial \varepsilon c_i}{\partial t} = -\nabla \cdot \underline{N}_i + a j_{in} + R_i \ . \qquad (3)$$

Here R_i is the rate of production of species i through homogeneous reactions and aj_{in} is the rate of production by means of the electrode reactions occurring throughout the volume of the porous electrode.

To a very good approximation, the solution is electrically neutral,

$$\sum_i z_i c_i = 0 \ , \qquad (4)$$

and the current density in an electrolytic solution is due to the motion of charged species:

$$\underline{i}_2 = F \sum_i z_i \underline{N}_i \ . \qquad (5)$$

For a porous electrode, we also need to mention that the current in the matrix phase is governed by Ohm's law:

$$\underline{i}_1 = -\sigma \nabla \Phi_1 \ . \tag{6}$$

The differential equations describing the electrolytic solution require boundary conditions for the behavior of an electrochemical system to be predicted. The most complex of these concerns the kinetics of electrode reactions. Electrode reaction j can be written symbolically as

$$\sum_i s_{ij} M_i^{z_i} \rightarrow n_j e^- \ , \tag{7}$$

thereby defining its stoichiometry. Then the normal component of the flux density of a species is related to the normal component of the current density, that which contributes to the external current to the electrode, according to Faraday's law:

$$j_{in} = - \sum_j \frac{s_{ij}}{n_j F} i_{nj} \ . \tag{8}$$

In equation 3, which has been averaged over the random geometry of a porous electrode, the term aj_{in} appears as an apparent production term in the solution-phase material balance for species i, a being the specific interfacial area.

The external electrode current is also obtained by summing the currents due to the individual electrode reactions:

$$\nabla \cdot \underline{i}_1 = -a \sum_j i_{nj} \ . \tag{9}$$

The surface overpotential for reaction j can be defined as the potential of the working electrode relative to a reference electrode of the same kind located just outside the diffuse double layer. For a porous electrode, we might express this in the form

$$\eta_{sj} = \Phi_1 - \Phi_2 - U_{jo} \ , \tag{10}$$

where

$$U_{jo} = U_j^{\theta} - U_{ref} - \frac{RT}{n_j F} \sum_i s_{ij} \ln \left(\frac{c_{io}}{\rho_o} \right) \ . \tag{11}^*$$

The solution potential Φ_2 is to be measured with a reference electrode of a given kind, and the equilibrium potential U_{jo} is expressed relative to the same reference electrode. For a situation where there are multiple electrode reactions, it would be inconvenient to have a multitude of solution potentials referred to different reference electrodes. Furthermore, it is unlikely that any reference electrode inserted directly into the solution could be equilibrated with respect to a certain electrode reaction, because of the presence of side reactions. In equation 10, ohmic potential drop and the diffusion potential between the wall and the bulk of the fluid in a pore are effectively ignored.

---

*In this equation, c_{io} should be expressed in moles per liter of solution.

One next needs to use a kinetic expression relating the current density to the surface overpotential and the species concentrations c_{io} at the wall:

$$i_{nj} = f_j(\eta_{sj}, c_{io}) \ , \tag{12}$$

where charging of the double layer is ignored. (Note that i_{nj}, η_{sj}, and c_{io} are all local quantities.) In the work described here, the Butler-Volmer equation was used:

$$i_{nj} = i_{oj}\left[\exp\left(\frac{\alpha_{aj}F}{RT}\eta_{sj}\right) - \exp\left(-\frac{\alpha_{cj}F}{RT}\eta_{sj}\right)\right] \ , \tag{13}$$

where i_{oj} depends on the species concentrations at the wall.

Within the porous electrode, mass transfer to the wall from the flowing solution is determined by the velocity profile in the detailed geometry of the porous structure. In the absence of a complete treatment of this problem, the fluxes at the surface are related to the wall concentrations by means of the local mass-transfer coefficient k_{mi}:

$$j_{in} = k_{mi}(c_{io} - c_i) \ . \tag{14}$$

A single-phase electrolytic solution is governed by similar equations, which are detailed elsewhere.[16] In equations 2 to 5, one can set $\varepsilon = 1$ and $a = 0$. The rotating-disk problem is typical of a large class where a partial separation between the mass-transfer problem and the potential-distribution problem can be made. Examples of such systems are shown in figures 1 and 4 to 7.

In these systems, concentration variations are restricted to thin layers adjacent to the surfaces of the electrodes, and Laplace's equation applies in the bulk of the solution outside these diffusion layers. This means that one can devote separate attention to these different regions. Since the diffusion layers are thin, the bulk region essentially fills the region of the electrolytic solution bounded by the walls of the cell and the electrodes. In this region the potential is determined so as to satisfy Laplace's equation and agree with the current density distribution on the boundaries of the region. In the diffusion layers, the concentrations are determined so as to satisfy the appropriate form of the transport equations, with a mass flux density at the wall appropriate to the current density on the electrodes (see equation 8) and approaching the bulk concentrations far from the electrode. The current distribution and concentrations at the electrode surface must adjust themselves so as to agree with the overpotential variation determined from the calculation of the potential in the bulk region (see equations 10 to 13).

The governing diffusion-layer equation for the concentration of a minor species reacting at a disk electrode rotating in a well-supported electrolyte can be solved to yield a relationship between the concentration and the flux density at the surface:

$$j_{in} = -D_i\left(\frac{a\nu}{3D_i}\right)^{1/3}\left(\frac{\Omega}{\nu}\right)^{1/2}\left\{\frac{c_{i\infty} - c_{io}(0)}{\Gamma(4/3)} - \frac{r}{\Gamma(4/3)}\int_0^r \frac{dc_{io}(x)}{dx}\,\frac{dx}{(r^3 - x^3)^{1/3}}\right\} \tag{15}$$

where x inside the integral denotes radial distance at points less than r. The simultaneous solution of this equation with i_{nj} given by equation 13, the Butler-Volmer form of the kinetic equation, and a potential obtained from Laplace's equation yields the desired current density distribution.

Results for the Rotating-disk Electrode

Figure 14 shows both the reaction distributions and the surface concentrations for one case of copper deposition at a rotating-disk electrode. Here the copper reaction is nearly at the limiting current (actually at 99.88 percent of limiting current). Hence, its reaction distribution is nearly uniform, and the concentration of cupric ions at the surface is lower by a factor of 166 at the edge than at the center, where it is already only one percent of the bulk value. The hydrogen reaction rate varies by a factor of about 164, and the surface concentration of dissolved hydrogen by a factor of about 65, between the center and the edge of the disk, where the local reaction rate amounts to about 54 percent of the copper deposition rate. On the average over the disk surface, the current efficiency for the copper deposition is about 94 percent. At the edge of the disk, the concentration of dissolved hydrogen exceeds its solubility by a factor of 9. Because of limited nucleation rates, one might speculate that we are on the verge of forming hydrogen bubbles.

The reason for the nonuniform distributions in figure 14 is seen in the distribution of the potential in figure 15. The potential in the solution varies by about 0.26 V from the center to the edge because of the nonuniform accessibility of the disk from an ohmic standpoint.

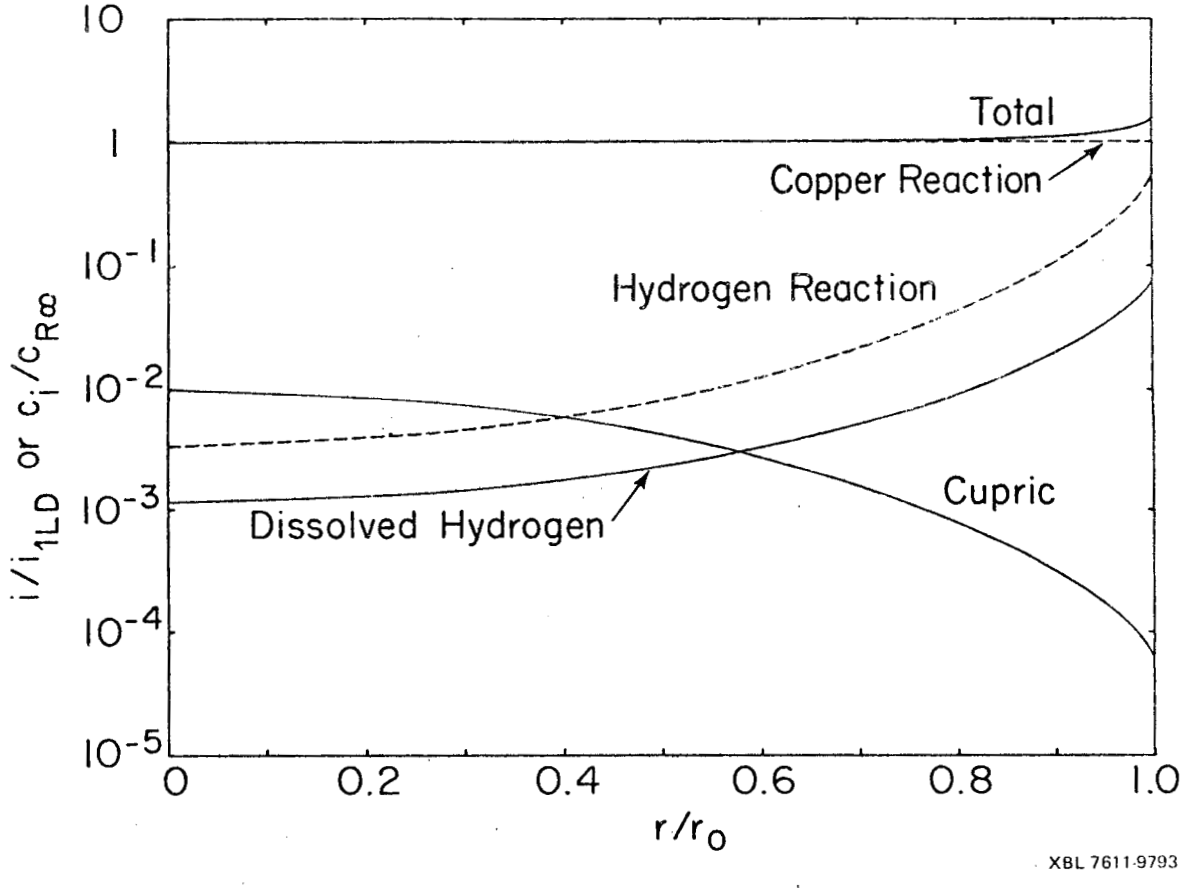

Figure 14. Current distributions, normalized with the limiting current density for copper deposition, and surface concentrations, normalized with the bulk cupric ion concentration, for reactions at a 5.74 cm diameter disk electrode rotating at 236 rad/s in a solution 0.1 M in $CuSO_4$ and 1.5 M in H_2SO_4 at 25°C. The H_2 saturation concentration is estimated to occur at $c_i/c_{R\infty} = 8.31\times10^{-3}$. This figure corresponds to a point at $V-\Phi_{ref} = -1.172$ V on figure 16.

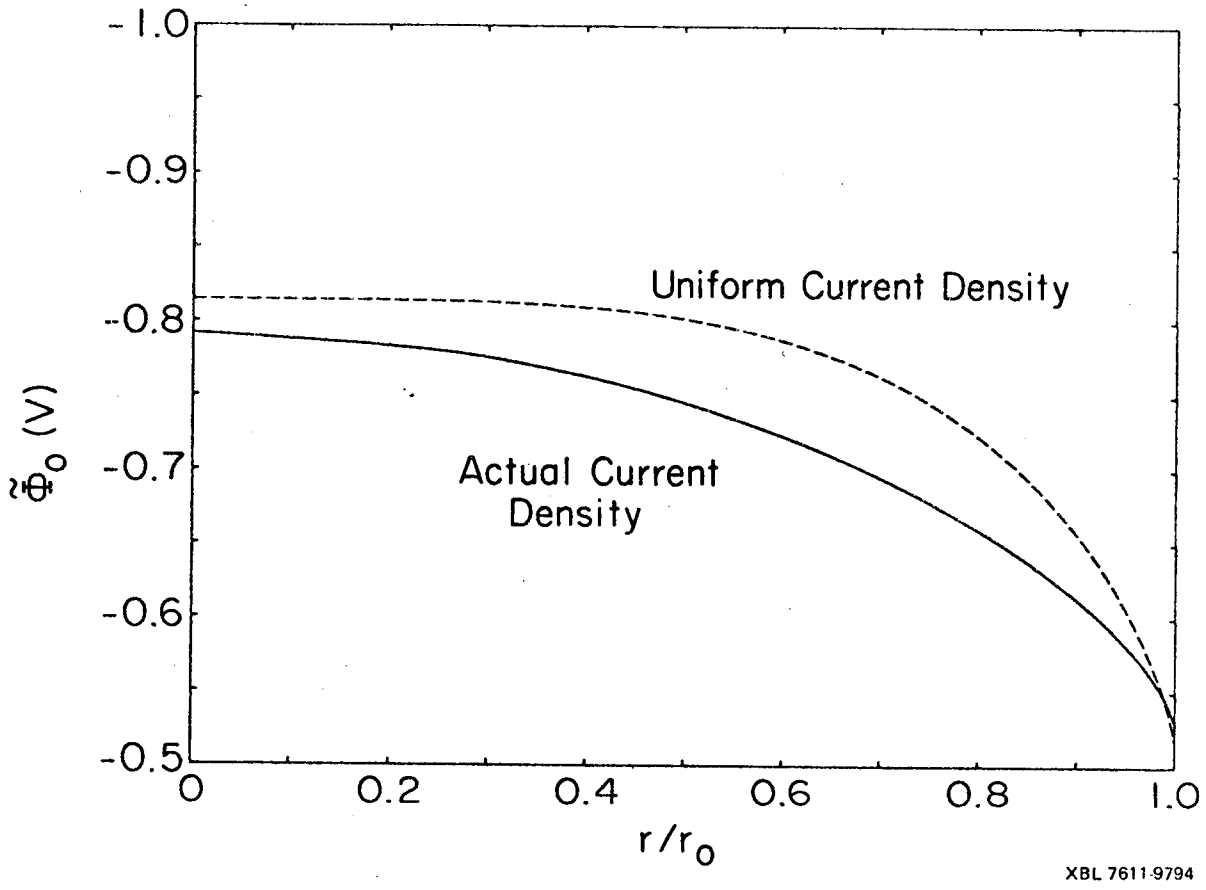

Figure 15. Distribution of $\tilde{\Phi}_o$, the potential calculated from the solution of Laplace's equation and extrapolated to the disk surface as though the conductivity were uniform and equal to the bulk value. The curves correspond to the same total current, that in figure 14, but with different distributions over the surface. For this total current, the primary distribution yields a constant value of $\tilde{\Phi}_o = -0.64$ V.

Figure 16 shows current-potential curves for a series of rotation speeds. The absence of a clearly defined limiting-current plateau is due to the occurrence of the side reaction. At sufficiently large driving forces, the nonuniform ohmic potential drop in solution can promote the onset of hydrogen evolution toward the edge of the disk, and this can occur before the attainment of a limiting-current condition at the center. Consequently, the plateau of the limiting-current curve for the deposition of copper is shortened and tilted, a phenomenon which becomes more pronounced as the rotation speed of the disk is increased.

Actually, one must pick somewhat extreme conditions of solution conductivity and disk size to illustrate the consequences of the nonuniform ohmic potential drop. With small disk electrodes and well supported solutions there is virtually no effect. However, the general importance of scale up in electrochemical engineering assures us that there are many practical systems in which the interaction of nonuniform ohmic potential drop and side reactions cannot be ignored.

Acknowledgment

This work was supported by the United States Energy Research and Development Administration. The author is grateful to James A. Trainham and Ralph White, two graduate students, for permission to use their results before the completion of their dissertations.

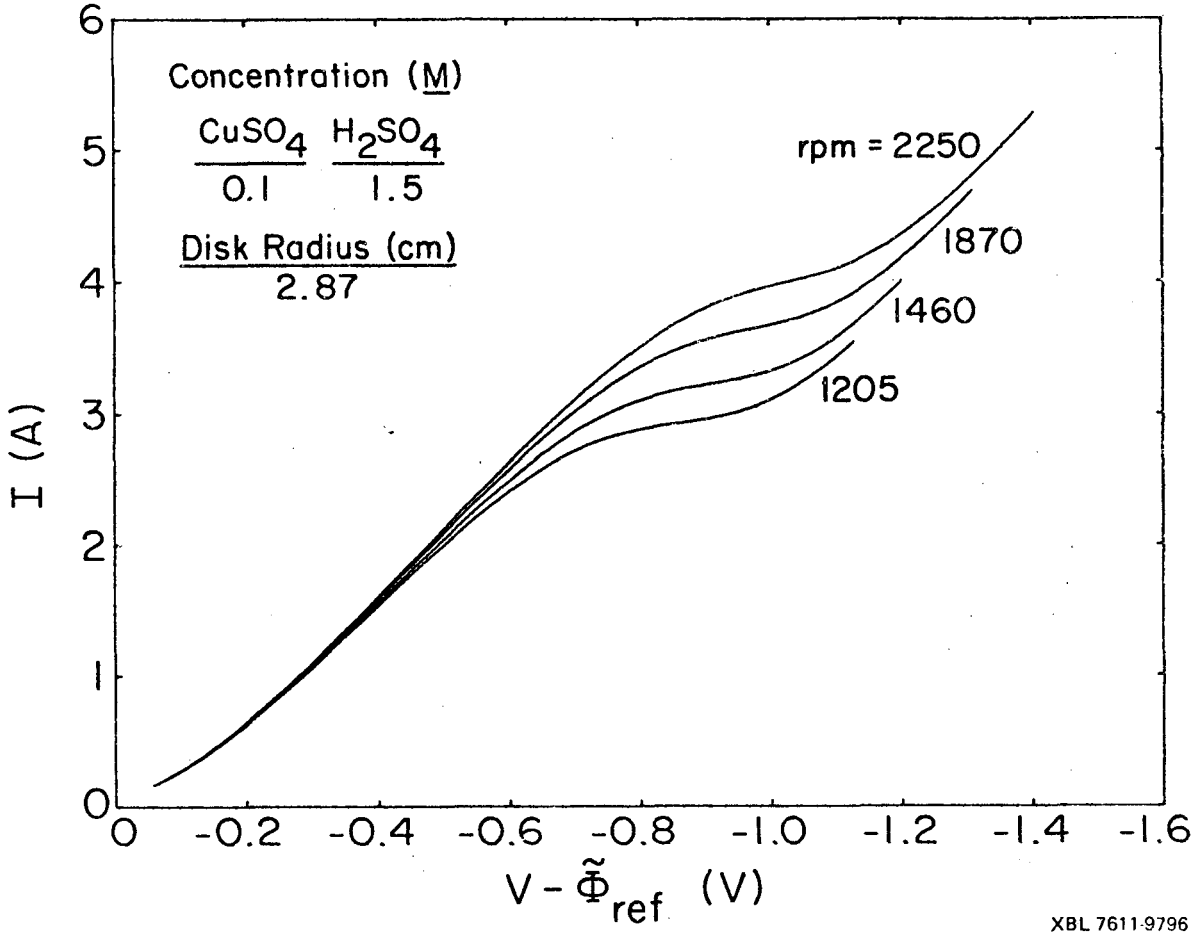

Figure 16. Current-potential curves for copper deposition on a rotating-disk electrode. The abscissa is the disk potential minus the potential of a copper reference electrode placed in the plane of the disk and 6.3 cm from the axis of rotation.

Nomenclature

a	specific interfacial area, cm^{-1}
a	0.51023, constant for the fluid mechanics of the rotating disk
c_i	concentration of species i, $mole/cm^3$
c_{io}	concentration of species i at the surface, $mole/cm^3$
$c_{i\infty}$	concentration of species i far from the disk, $mole/cm^3$
c_R	concentration of principal reactant, cupric ions, $mole/cm^3$
c_{Rf}	feed concentration of principal reactant, $mole/cm^3$
D_i	effective diffusion coefficient of species i, cm^2/s
D_o	diffusion coefficient of principal reactant in a free solution, cm^2/s
e^-	symbol for the electron
f_j	current density for reaction j, A/cm^2
F	Faraday's constant, 96,487 C/equiv
h	distance between two electrodes in a flow channel, cm
i	current density, A/cm^2
$\underline{i}_1$	superficial current density in matrix phase, A/cm^2
$\underline{i}_2$	superficial current density in solution phase, A/cm^2
i_{lLD}	limiting current density for copper deposition, A/cm^2
i_{nj}	normal component at an electrode of the current density for reaction j, A/cm^2
i_{oj}	exchange current density for reaction j at concentrations c_{io}, A/cm^2
i_{avg}	average current density to an electrode, A/cm^2
I	total current to an electrode, A
j_{in}	normal component at an electrode of the flux density of species i, $mole/cm^2$-s

k_m mass-transfer coefficient, cm/s

k_{mi} local mass-transfer coefficient, cm/s

L length or thickness of electrode, cm

M_i symbol for the chemical formula of species i

n_j number of electrons transferred in reaction j

$\underline{N}_i$ superficial flux density of species i, mole/cm^2-s

r radial distance on a disk electrode, cm

r_o radius of disk electrode, cm

R universal gas constant, 8.3143 J/mole-K

R_i production rate of species i in homogeneous chemical reactions, mole/cm^3-s

s_{ij} stoichiometric coefficient for species i in reaction j

t time, s

T absolute temperature, K

u_i effective mobility of species i, cm^2-mole/J-s

U_{jo} theoretical open-circuit potential for reaction j, V

U_j^θ standard electrode potential for reaction j, V

v superficial fluid velocity, cm/s

<v> average velocity in a flow channel, cm/s

VOP potential of porous electrode matrix relative to a downstream calomel electrode, V

x distance along an electrode from its upstream end, cm

z_i valence or charge number of species i

α_{aj} anodic transfer coefficient for reaction j

α_{cj} cathodic transfer coefficient for reaction j

$\Gamma(4/3)$ 0.89298, the gamma function of 4/3

ε porosity or void volume fraction of porous electrode

η overpotential, V

η_{sj} surface overpotential for reaction j, V

θ angular position on rotating sphere

κ solution conductivity, $ohm^{-1}-cm^{-1}$

ν kinematic viscosity of solution, cm^2/s

ρ_o density of pure solvent, g/cm^3

σ effective conductivity of matrix phase, $ohm^{-1}-cm^{-1}$

$\tilde{\Phi}_o$ potential in the solution extrapolated to the disk surface, V

Φ_1 matrix-phase potential, V

Φ_2 solution-phase potential, V

Ω rotation speed, radian/s

References

1. Carl Wagner. "The Scope of Electrochemical Engineering." Charles W. Tobias, ed. Advances in Electrochemistry and Electrochemical Engineering, 2 (1962), 1-14.

2. Jan Robert Selman and John Newman. "Free-Convection Mass Transfer with a Supporting Electrolyte." J. Electrochem. Soc., 118 (1971), 1070-1078.

3. N. Ibl. "The Use of Dimensionless Groups in Electrochemistry." Electrochim. Acta, 1 (1959), 117-129.

4. W. R. Parrish and John Newman. "Current Distributions on Plane, Parallel Electrodes in Channel Flow." J. Electrochem. Soc., 117 (1970), 43-48.

5. W. R. Parrish and John Newman. "Current Distribution on a Plane Electrode below the Limiting Current." J. Electrochem. Soc., 116 (1969), 169-172.

6. John Newman. "Current Distribution on a Rotating Disk below the Limiting Current." J. Electrochem. Soc., 113 (1966), 1235-1241.

7. Peter Pierini, Peter Appel, and John Newman. "Current Distribution on a Disk Electrode for Redox Reactions." J. Electrochem. Soc., 123 (1976), 366-369.

8. Kemal Nişancioğlu and John Newman. "Current Distribution on a Rotating Sphere below the Limiting Current." J. Electrochem. Soc., 121 (1974), 241-246.

9. Kameo Asada, Fumio Hine, Shiro Yoshizawa, and Shinzo Okada. "Mass Transfer and Current Distribution under Free Convection Conditions." J. Electrochem. Soc., 107 (1960), 242-246.

10. Richard Alkire and Ali Asghar Mirarefi. "The Current Distribution Within Tubular Electrodes under Laminar Flow." J. Electrochem. Soc., 120 (1973), 1507-1515.

11. Douglas N. Bennion and John Newman. "Electrochemical removal of copper ions from very dilute solutions." J. Appl. Electrochem., 2 (1972), 113-122.

12. Peter W. Appel and John Newman. "Application of the Limiting-Current Method to Mass Transfer in Packed Beds at Very Low Reynolds Numbers." AIChE J., to be published.

13. Douglas N. Bennion. "Flow Through Porous Electrodes for Removal of Ions from Dilute Solutions." Paper No. 69. Extended Abstracts. 27th meeting, International Society of Electrochemistry, Zürich, Switzerland, September 6-11, 1976.

14. John Newman and William Tiedemann. "Porous-Electrode Theory with Battery Applications." AIChE J., 21 (1975), 25-41.

15. John Newman and William Tiedemann. "Flow-through Porous Electrodes." Advances in Electrochemistry and Electrochemical Engineering, to be published.

16. John S. Newman. Electrochemical Systems. Englewood Cliffs, N.J.: Prentice-Hall, Inc., 1973.